3D Printing of Magnetoresponsive Polymeric Materials with Tunable Mechanical and Magnetic Properties by Digital Light Processing

3D printing of Magneto-Responsive Polymeric Materials with Tunable Mechanical and Magnetic Properties by Digital Light Processing (DLP)

Simone Lantean[1,2], Gabriele Berra[3], Candido Fabrizio Pirri[1,4], Paola Tiberto[3], Marco Sangermano[1], Ignazio Roppolo[1]*, and Giancarlo Rizza[2]

[1]Department of Applied Science and Technology, Politecnico di Torino, Corso Duca degli Abruzzi 24, 10129, Torino, Italy

[2]Laboratoire des Solides Irradiés (LSI), Ecole Polytechnique, CEA/DRF/IRAMIS, CNRS, Route de Saclay, 91128 Palaiseau Cedex, France

[3]Advanced Materials for Metrology and Life Sciences Division, INRiM, Strada delle Cacce 91, 10143 Torino, Italy

[4] Center for Sustainable Future Technologies @Polito, Istituto Italiano di Tecnologia, Via Livorno, 60, 10144, Torino, Italy

e-mail: ignazio.roppolo@polito.it

Abstract

In this work the Digital Light Processing (DLP) technique has been used for printing of magneto–responsive polymeric materials with tunable mechanical and magnetic properties. Mechanical properties were tailored, from stiff to soft, by combining urethane-acrylate resins with butyl acrylate reactive diluent, while the magnetic response of the printed samples was tuned by changing the Fe_3O_4 nanoparticle loading up to 6 wt%. Following this strategy, we implement the DLP processes to fabricate magneto-responsive active components with programmable complex functions using external magnetic fields. Our approach has been demonstrated/validated by probing different kind of movements, such as the rolling, the translation, the stretching, the shapeshifting and the folding / unfolding, on a large panel of printed objects with varying stiffness and magnetic responses.

1. Introduction

Bringing the dynamics of the life into unanimated objects is the new realm of the additive manufacturing. This novel mindset is called “4D printing” and aims at using advanced materials responding to the influence of external stimuli or energy to program the actions of the printed object (*1-4*). So far, different stimuli-responsive materials – e.g. electroactive polymers (*5-7*), hydrogels (*8-11*) and nanocomposites (*12-15*)- have been investigated for a broad variety of applications spanning from micro and soft robotics (*10, 16-18*) to biomedicine (*19-22*). Among the different strategies, an accessible pathway to fabricate stimuli-responsive (4D) printed objects is to fabricate a magnetic-responsive material by loading the polymeric matrix with magnetic fillers, as magnetite (Fe_3O_4) or neodymium-iron-boron (NdFeB) particles (*24-30*). In the wake of this idea, so far Direct Ink Writing (DIW) and Fused Filament Fabrication (FFF) have been used

to fabricate fast responding actuators (*23, 31, 32*), inks containing high load of magnetic fillers (*33*) and 2D planar structures exploiting folding and unfolding processes (*34*). However, both DIW and FFF present limitations in term of detail resolution of the final object, dispersion of the fillers – that may lead to a non-homogeneous magnetic response- and processing temperature (*35*). For the latter, these drawbacks can, in principle, be avoided by using additives to decrease the processing temperature. However, this approach drastically impacts on the mechanical performances of the printed devices (*33*).

An alternative to DIW and FFF approaches is the Digital Light Processing (DLP) technique. This vat polymerization 3D printing technology involves the use of photosensitive (liquid) resins which are able to cure (solidify) upon irradiation with a suitable light source. In the DLP, a digital light projector (micro-mirror device) illuminates a photocurable resin with a two-dimensional pixel pattern allowing the curing of single slice of the 3D object (36, *37,38*). The use of the DLP technique allows to overcome the aforementioned drawbacks associated to DIW and FFF. Indeed, i) the printing resolution in DLP is related to the pixel dimension and it is generally higher than that of DIW and FFF, (*39, 40*), ii) as in DLP a liquid formulation is used, the dispersion of the fillers is easier to control, and iii) the fabrication process generally occurs at room temperature. Nevertheless, two main precautions must be taken into account: first, fillers and photoinitiators compete in absorbing the incident radiation, thus increasing the loading content of nanoparticles may affect the photopolymerization process. Second, to print an object which responds homogeneously to an external input, the dispersion of the fillers must be stable for the whole printing procedure, thus macroscopic sedimentation, segregation and spatial inhomogeneities must be avoided.

Recently, some works have been published on the use of DLP to print magnetic nanocomposite materials. Among them Martin *at al.*, (*43*), demonstrated the possibility to print bioinspired reinforced materials controlling the orientation of alumina platelets decorated with magnetite nanoparticles, while Ji and coworkers showed the possibility to print multilayered magnetic soft-actuators containing 1 wt.% of magnetite nanoparticles (*44*).

Following this strategy, in this work we applied DLP technology to fabricate magnetic responsive soft objects with programmable complex functions, and magneto-responsive active components, (*23*). The desired mechanical properties and the functional response of the object is obtained by optimizing the photocurable formulation both in terms of reactivity and mechanical properties. This is based on our previous knowledge in printing polymer nanocomposites containing nanostructures (see e.g. *41, 42)*. In particular, mechanical response of the printed polymeric matrix is tailored from stiff to a flexible material by combining urethane-acrylated resins with butyl acrylate employed as reactive diluent. Using optimized formulations and a visible light as a photocuring source, we were able to load the resin up to 8% wt of magnetite nanoparticles. Finally, as a proof of concept, we fabricate a set of high resolution 3D objects with complex shapes whose movements can be controlled by the application of an external magnetic field.

2. Experimental

2.1 Materials

Ebecryl 8232 (Eb), a urethane-acrylated resin was kindly provided by Allnex, butyl acrylate (BA) was purchased from Merck and added to Eb in several weight ratios as a reactive diluent. Phenylbis(2,4,6-trimethylbenzoyl)phosphine oxide (Merck) was added to the formulation as photoinitiator at 1 wt.% of the monomers. Spherical shape magnetite (Fe_3O_4) nanoparticles with nominal diameter ranging between 50-100 nm (98% purity) were purchased from Merck and used as received.

2.2 Formulation preparation

Several formulations were prepared varying the amount of the reactive diluent (BA) and the concentration of Fe_3O_4 nanoparticles (Table 1). BA was added to Ebecryl 8232 in three different weight concentration (0%, 25% and 50%), resulting in three different formulations named 100Eb, 75Eb25BA and 50Eb50BA, respectively. For each formulation, the concentration of the loaded Fe_3O_4 NPs was increased from 0 to 8 wt% relative to the amount of monomers. In the end, the photoinitiator was added to the formulation at 1 wt.% of monomers amount. Formulations were then stirred to homogenize the distribution of both photoinitiator and magnetite nanoparticles. Also, before printing, or any further characterization, formulations were sonicated for 10 minutes in order to both disaggregate particles and to improve their dispersion and to homogenize the photocurable resin.

Table 1: Formulations' composition(*).

Sample	Ebecryl 8232 (wt.%)	Butyl Acrylate (wt.%)	Fe_3O_4 nanoparticles (wt.% of monomers)
100Eb	100	/	0
75Eb25BA	75	25	0
75Eb25BA_2NPs	75	25	2
75Eb25BA_4NPs	75	25	4
75Eb25BA_6NPs	75	25	6
75Eb25BA_8NPs	75	25	8
50Eb50BA	50	50	0
50Eb50BA_2NPs	50	50	2
50Eb50BA_4NPs	50	50	4
50Eb50BA_6NPs	50	50	6
50Eb50BA_8NPs	50	50	8

(*) all the formulations contained 1 wt% of the photoinitaitor with respect to the amount of monomer.

2.3 3D-printed Sample preparation

The formulations were 3D-printed using a RobotFactory HD 2.0 DLP printer equipped with a broad band projector emitting in the visible range, with 10 mW/cm^2 of intensity and a nominal resolution of 50 μm in the x-y plane, while the maximum resolution in z direction was 10 μm. In order to improve the adhesion of the printed structures to the building platform, a base-layer depleted of Fe_3O_4 NPs was fabricated before the printing of the final

object. After samples cleaning, specimens underwent a UV post-curing for 10 minutes, performed with a medium-pressure mercury lamp also provided by RobotFactory.

2.4 Characterization

FT-IR spectra were collected using a Nicolet 50 FT-IR (Thermo Scientific). Formulations were coated on a silicon wafer using a wire wound bar, the film thickness was 12 μm. Samples were irradiated for 0, 10, 20 and 30 s using a Hamamatsu LC8 visible lamp with a cut-off filter below 400 nm, at the intensity of 10 mW/cm^2 and under nitrogen flux. The conversion ratio of the acrylic groups was investigated monitoring the decrease of double-bond peak area at 1630-1650 cm^{-1} during irradiation normalized with the aromatic peak area (1505-1575 cm^{-1}).

Rheological tests were performed with an Anton Paar rheometer (Physica MCR 302). The gap between the plates was settled at 0.2 mm, and the shear rate was varied from 0.1 to 100 1/s. The same instrument was also used to perform photo-reological tests. In this case the machine was equipped with a Hamamatsu LC8 lamp having a cut-off filter below 400 nm and an intensity of 10 mW/cm2. The gap between the plates was 0.2 mm, and, to stabilize the system, light was switched on after 60s. The tests were performed under constant temperature (25°C) and shear frequency (1 rad/s).

Dynamic mechanical thermal analysis (DMTA) was performed with Triton Technology TTDMA. 3D printed samples were tested in strain control (0.02 mm of strain) with a frequency of 1Hz, from -50°C to 40°C with a ramp rate of 3°C/min. Parallelepiped-shape specimens (40x5x2 mm) were first 3D printed and tested. Glass Transition Temperature

(T_g) were set as maximum of tan δ (= E''/E'). Stress-strain tests were performed with the same equipment to investigate the mechanical properties of the material. For each formulation, four samples were tested at room temperature and with a load rate of 1 N/min. Optical microscopy images were taken with Olympus BX53 M microscope. The ocular lenses and the objective lenses were equipped with 10x magnification.

Field emission scanning electron microscope (FESEM, Zeiss Supra 40) has been used to investigate the dispersion, distribution and agglomeration of magnetite NPs in 3D printed samples changing their concentration and the viscosity of the former formulations. The investigated surfaces were obtained by cryofracture of specimens.

Room-temperature hysteresis loops of 3D printed samples were measured by means of a Vibrating Sample Magnetometer (VSM, Lakeshore 7400). The samples were mounted on a quartz sample-holder rod and submitted to a magnetic field (H) ranging in the interval -17 kOe < H < 17 kOe. The magnetometer is routinely calibrated by means of a standard nickel sphere.

3. Results and discussion

3.1 Optimization of the photocurable resin containing magnetic nanofillers

Magneto-responsive polymers are obtained by loading Ebecryl 8232 (100Eb) resin with Fe_3O_4 nanofillers. Besides, a reactive diluent (butyl acrylate, BA) was added to tune the viscosity of the resins, the reactivity of the formulations towards light irradiation and the mechanical properties of

the printed objects. As shown in Figure 1a, the addition of 25 wt% BA to pure Ebecryl (75Eb25BA), results in a decreasing of the viscosity by one order of magnitude, i.e. from 5.06 to 0.18 Pa·s. This value is further reduced by another one order of magnitude when the concentration of BA is increased to 50 wt% (50Eb50BA), i.e. at 0.02 Pa·s. However, for higher concentration of BA the viscosity becomes so low that segregation/sedimentation effects makes the correspondent formulations instable and not suitable for our purposes. For all the formulations, the successive addition of magnetic nanofillers up to a concentration of 8 wt%, do not significantly affect the final viscosity (see Figure 1a). This unexpected result can be explained by considering the lubricant effect of spherical magnetite particles, which counterbalance the viscosity enhancement due to the fillers dispersion (33).

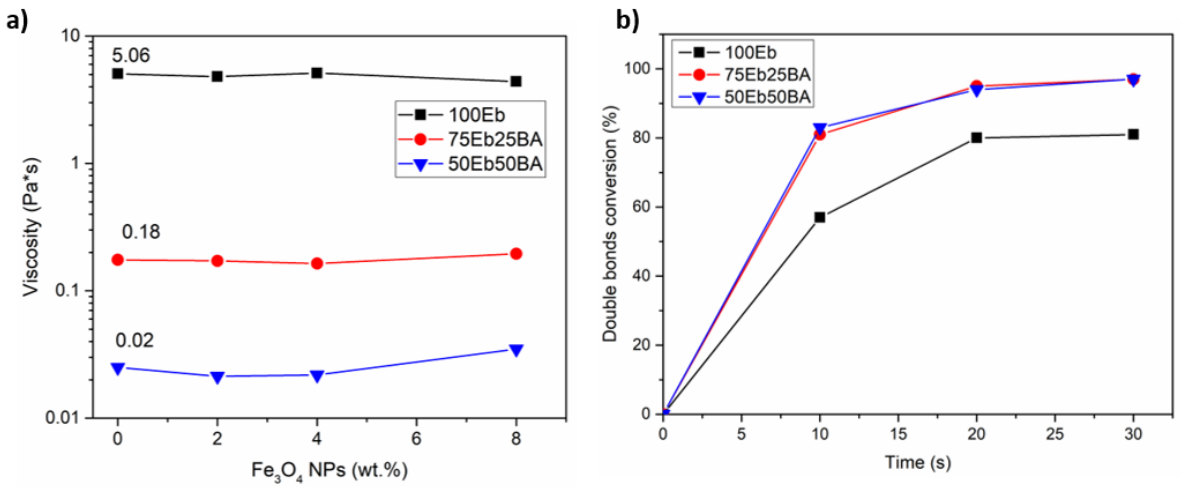

Figure 1: a) Influence of BA and NPs on formulation's viscosity. b) Double bond conversion VS irradiation time of 100Eb, 75Eb25BA and 50Eb50BA formulations.

To guarantee the homogeneous response of the printed objects, magnetite NPs dispersed within the formulations must be stable during the overall printing process. Otherwise stated, sedimentation and agglomeration processes must be avoided. Thus, the temporal stability of the embedded nanofillers was investigated. As a general result, we obtain that all the formulations are stables, i.e. no sedimentation nor agglomeration of the nanofillers are observed, for at least 1h which is compatible with the printing process. As an example, in figure S1 (Supporting Information) we show the stability of the formulation 50Eb50BA_6NP, which presents the lowest viscosity and the maximum amount of loaded Fe_3O_4 nanofillers, i.e. 6% wt.

Next, we evaluate the reactivity of the photopolymerization process of the Ebecryl formulations modified by the presence of the reactive diluent (BA) and the magnetic nanonfillers. In Figure 1b the double bonds conversions are reported as a function of irradiation time for different concentrations of the BA, i.e. 0 wt% (100Eb), 25 wt% (75Eb25BA), and 50 wt% (50Eb350BA). The corresponding collected spectra are reported in Supporting Information (Figure S2-S4). The pristine Ebecryl resin (100Eb) shows an overall double bond conversion of about 80% after 20 sec. The 75Eb25BA formulation reaches about 95% and it is accompanied by an enhancement of photopolymerization rate. This phenomenon, also known as viscosity effect (*38*, *45*), is associated to the presence of a low viscous reactive diluent that postpones the gelation point, which in turn accelerates the polymerization kinetics and increases the double bond conversions. However, when the BA content is further increased up to 50 wt%, not significant effects are visible, Figure 1b. Due to the higher reactivity, only the formulations containing BA are considered for the following investigations.

The influence of magnetic nanofillers (up to 8 wt%) on the polymerization process was evaluated by photorheology tests, by following the evolution of the storage moduli with the irradiation time. This is shown in Figure 2a-b for the 75Eb25BA formulation and in Figure 2c-d for the 50Eb50BA formulation. In agreement with FT-IR measurements, no appreciable differences between 75Eb25BA and 50Eb50BA formulations (without NPs) were observed. Indeed, in both cases, a fast photopolymerization process takes place as soon as the light is switched on. On the other hand, the addition of Fe_3O_4 nanoparticles causes in both the mixtures a slight delay in photopolymerization (see magnification of the starting point, Figure 2b and Figure 2d), which scales with the concentration of the nanofillers. This effect can be explained by considering the existence of a competitive absorption between the photoinitiator and the nanopowders. The efficiency of the radical photo-initiator is described by two quantum yields: the *quantum yields of initiation*, which represents the number of activated polymeric chains per absorbed photon, and the *quantum yields of polymerization*, which represents the number of monomer units polymerized per absorbed photon. (*46-48*) In presence of additional absorption sites, i.e. the ceramic nanofillers, the amount of the photons absorbed by the photoinitiator is reduced, which in turn leads to a decrease of the quantum yields and therefore to the slowing of the reaction kinetics. Despite the slight decrease of photoreactivity, we were able to increase the concentration of embedded nanofillers up to 8 wt%, a greater value compared to the literature. (*44*) This could be explained considering that magnetite NPs have a lower absorption coefficient in the visible range (about $2x10^5$ cm^{-1}) than in UV-range (about $5x10^5$ cm^{-1}). (*49*) It is important to evidence that the parameters extrapolated from photorheology experiments cannot be directly used for 3D printing

procedure (e.g. irradiation time vs gel point), however those measurements give us useful indication for optimizing the printing process.

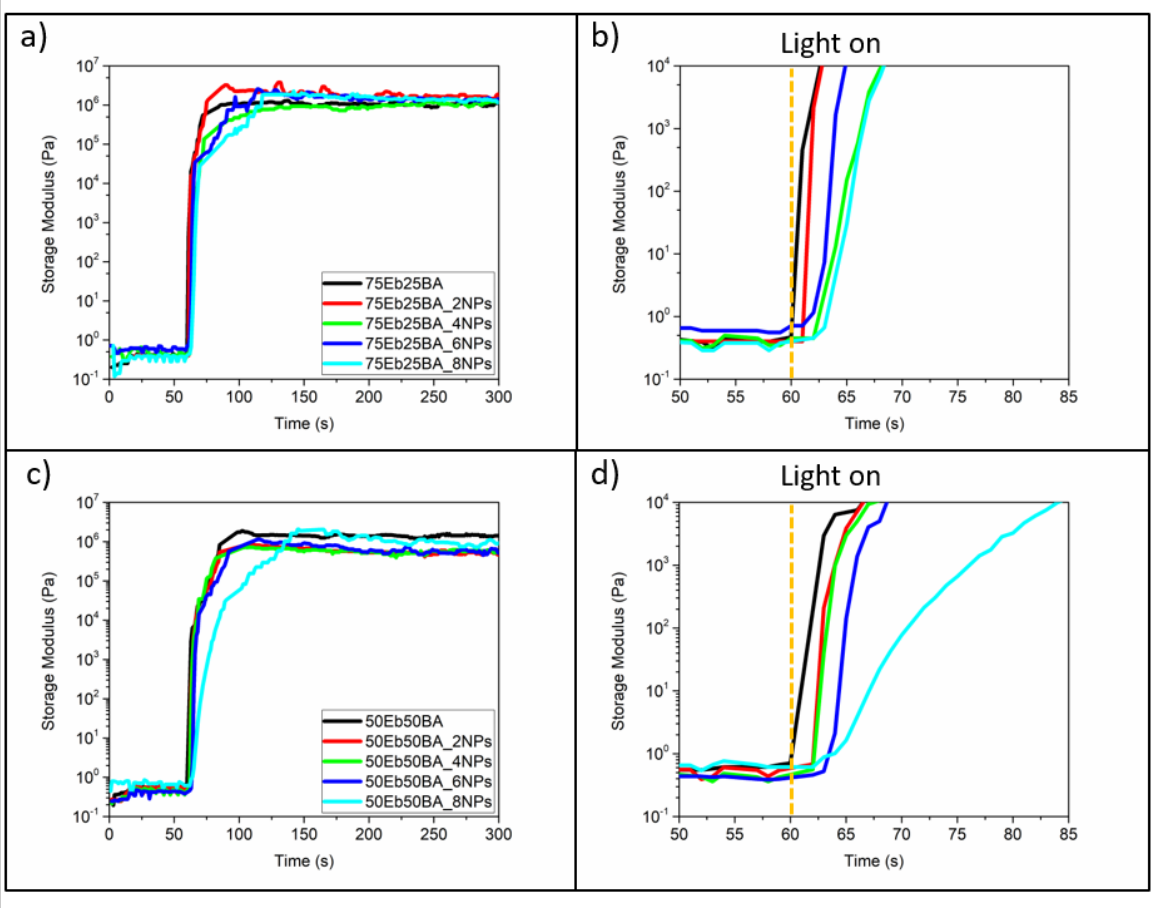

Figure 2: a) Photoreology tests performed on 75Eb25BA formulations. b) Zoom in during the first minutes of radiation of 75Eb25BA formulations. c) Photoreology tests performed on 50Eb50BA formulations. d) Zoom in during the first minutes of radiation of 50Eb50BA formulations.

3.2 3D-printing of the optimized photocurable formulation and material characterization

First, to enhance the adhesion between the nanocomposite and the printing platform, a layer of polymer without nanofillers is pre-printed. Then, formulations containing Fe_3O_4 NPs at increasing concentrations, up to maximum of 8 wt.%., are processed setting the minimum thickness for each slice at 20 μm. The processing parameters are reported in Table 2. As expected, increasing the NPs content results in an increasing of the irradiation time, following an exponential law (Figure 3a and 3b). Dataset can be fitted by the equation:

$$y = A \cdot e^{x/t} + y_0 \quad \text{(eq. 1)}$$

The fitted curves are used to extrapolate the processing time and to check if it is compatible with the DLP (maximum irradiation time per layer 20s). According to the interpolation curves, it could be possible to print nanocomposites with up to 12%wt of Fe_3O_4 NPs. Howere, taking into account that the mechanical resistance of the sample deteriorates with the NPs concentration (see Figure 3c), we fixed the maximum amount of loaded magnetic nanofillers at 6 wt%.

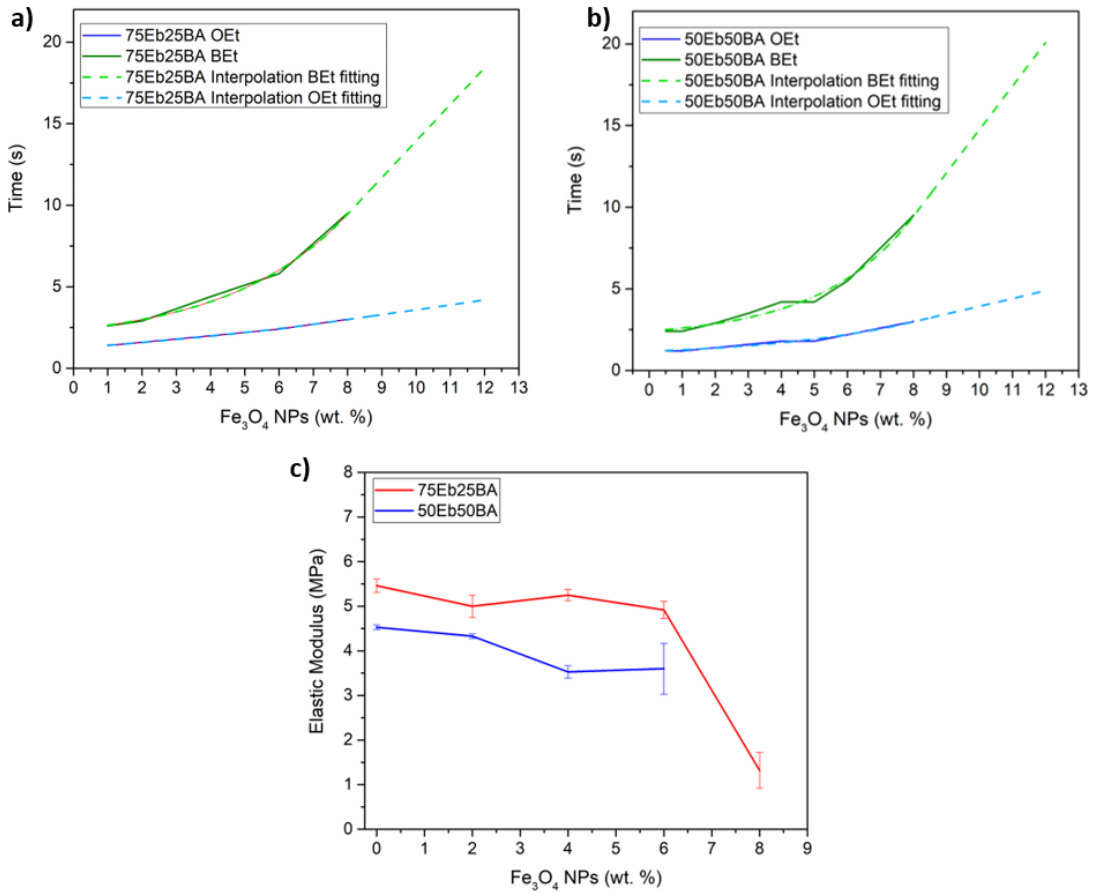

Figure 3: DLP processing parameters and their interpolation curves at several NPs concentrations of: a) 75Eb25BA formulation and b)50Eb50BA formulation. c): Elastic moduli trends when NPs concentrations is increased.

Dynamic Mechanical Thermal Analysis (DMTA) is used to evaluate the thermo-mechanical properties of the 3D printed samples. The influence of BA and Fe_3O_4 NPs on the glass transition temperature (T_g) of the 3D printed samples was determined (Table 2). The tan δ curves are shown in Figures S5 e S6 in Supporting Information for the Eb75BA25 and Eb50BA50 formulations, respectively. On one hand, when BA is added to the photocurable formulations, the T_g of the cross-linked material decreases. This softening effect is related to two phenomena: first a decrease of

cross-linking density due to the presence of a monofunctional monomers, second to the low T_g (about -51 °C) of the polybutylacrylate (*50*). On the other hand, the T_g for the cross-linked material is observed to slightly decrease up to 4 wt.% of magnetite nanoparticles, above this value the reduction of T_g is more marked. At first glance, this behavior can be ascribed to both the reduction of double bond conversion, in turn related to the competitive absorption, and to the lubricating effect (*51*).

Mechanical properties of the printed samples were evaluated by performing stress-strain tests on the printed objects using the 100Eb samples for reference. For the formulations without nanofillers, Figure 3c shows that the elastic modulus (E) decreases when BA is added, e.g. passing from 7 MPa for 100Eb to 5.5 MPa for 75Eb25BA to 4.5 MPa for 50Eb50BA. For the nanocomposites, we observed a similar trend for both 75Eb25BA and 50EB50BA samples. In both formulations, that values of E slightly decrease up to 6 wt% of nanofillers. Above this value, a large drop of E was measured for 75Eb25BA samples. This is probably related to the defects produced during the manufacturing process. The sample 50Eb50BA_8NPs was not printable due to its poor mechanical properties. Thus, by considering both mechanical properties and printing limitations, we set at 6 wt% the maximum concentration of nanofillers for the fabrication of our magneto-responsive polymers.

Table 2: Process parameters and glass transition temperatures of all studied formulations.

SAMPLE	Slicing (μm)	Base exposing time (s)	Object exposing time (s)	T_g (°C)
100Eb	50	2.2	1.6	19.7
100BA		Not printable		-51.6(*50*)
75Eb25BA	50	2	1	4.3
75Eb25BA_2NPs	20	2.9	1.6	3.1
75Eb25BA_4NPs	20	4.4	2	3.3
75Eb25BA_6NPs	20	5.8	2.4	1
75Eb25BA_8NPs	20	9.5	3	-11
50Eb50BA	50	2	1	-6.2
50Eb50BA_2NPs	20	2.9	1.4	-8.4
50Eb50BA_4NPs	20	4.2	1.8	-7
50Eb50BA_6NPs	20	5.5	2.2	-10.7
50Eb50BA_8NPs	20	9.5	3	Not measured

The dispersion of the embedded magnetic nanoparticles is analyzed by optical and scanning electron (FESEM) microscopies (Figure 4). Optical analysis is performed on thin films, 12 μm thick, coated on a microscope slide by wire wound bar. FESEM images were taken on the cryo-fractured surfaces of 3D printed samples. To study the influence of viscosity on NPs dispersion, four systems were investigated: 75Eb25BA_2NPs, 75Eb25BA_8NPs, 50Eb50BA_2NPs and 50Eb50BA_6NPs. In all the samples but 50Eb50BA, a homogeneous distribution of magnetite nanoparticles was observed. For the latter, some aggregates are visible, probably due to the low viscosity of this system, which makes difficult the homogeneous dispersions of the nanofillers.

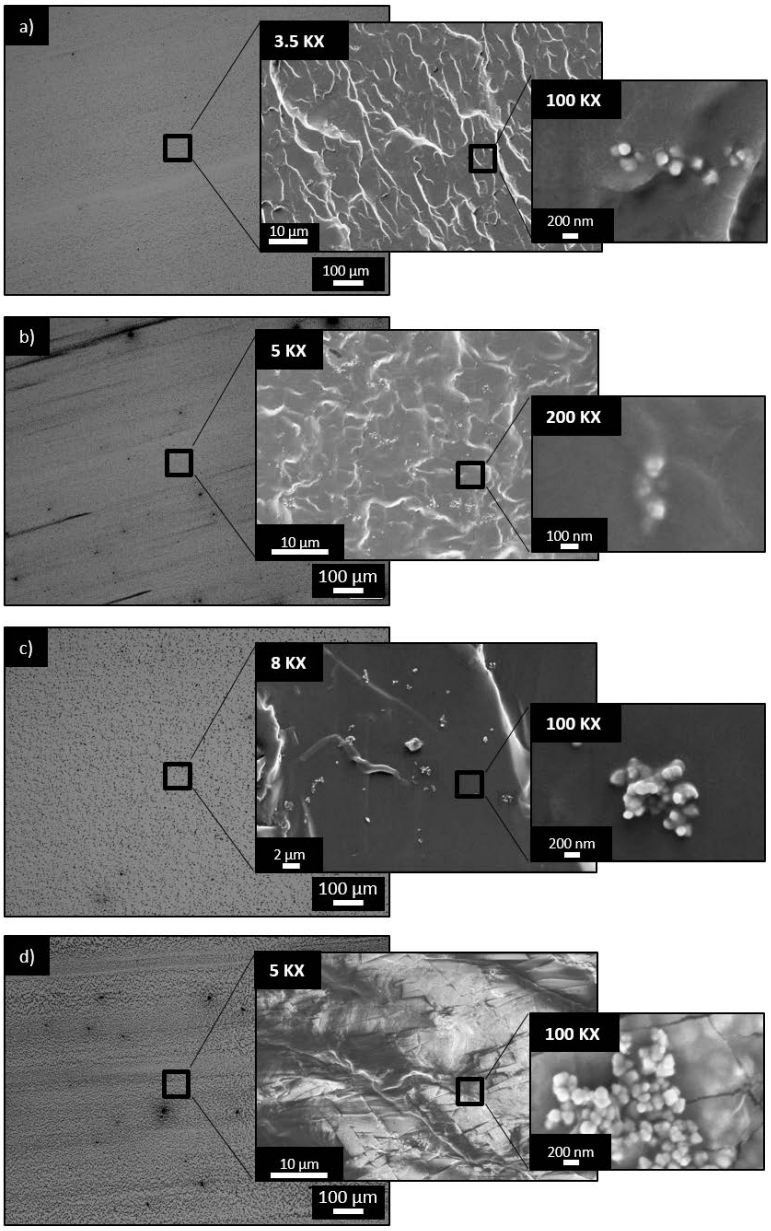

Figure 4: Optical microscope images taken of 75Eb25BA_2NPs (a), 75Eb25BA_8NPs (b), 50Eb50BA_2NPs (c) and 50Eb50BA_6NPs (d) formulations. On the inserts, FESEM images at different magnification values are reported.

3.3 Magnetic properties of the 3D printed samples

Room-temperature hysteresis loops are reported in Figures 5a and 5b for 75Eb25BA and 50Eb50BA samples, respectively, for different nanofiller concentrations. The latter value has been estimated by TGA measurements, and shown in Figures S7 and S8 of Supporting Information. The magnetization (M) of the 3D printed nanocomposites is obtained by normalizing the magnetic moment to the sample mass. Magnetization curves display the same hysteretic and reversal behavior, fully compatible with Fe_3O_4 particles having 50-100 nm diameter and in multi-domain state. As expected, M increases with increasing Fe_3O_4 content independently from the matrix formulation. This behavior is confirmed in Figure 5c for the two samples (5Eb25BA squares and 50Eb50BA circles) where a linear behavior between the value of M, taken at the maximum applied field (H = 17 kOe), and the nanoparticles concentration is observed. Besides, a coercivity value of ~ 120 Oe has been recorded in all studied samples indicating that the magnetic volume coherently responding to an external magnetic field H is substantially equal in the two class of 3D polymers (*52*). This result suggests a homogeneous distribution of Fe_3O_4 nanoparticles in the polymer matrix with a small fraction of NP aggregates confirming the analysis of optical and electronic images.

The magnetic force F_{mag} exerted on the magnetic polymer by applying an external magnetic field gradient to control the translation motion is given by:

$$F_{mag} = MV\nabla H \qquad \text{(eq. 2)}$$

where M is magnetization, V is the sample volume and ∇H is the external field gradient.

The hysteresis curve maps the magnetic response as a function of the external magnetic field and consequently allows to figure out the F_{mag} intensity for all studied polymer concentration.

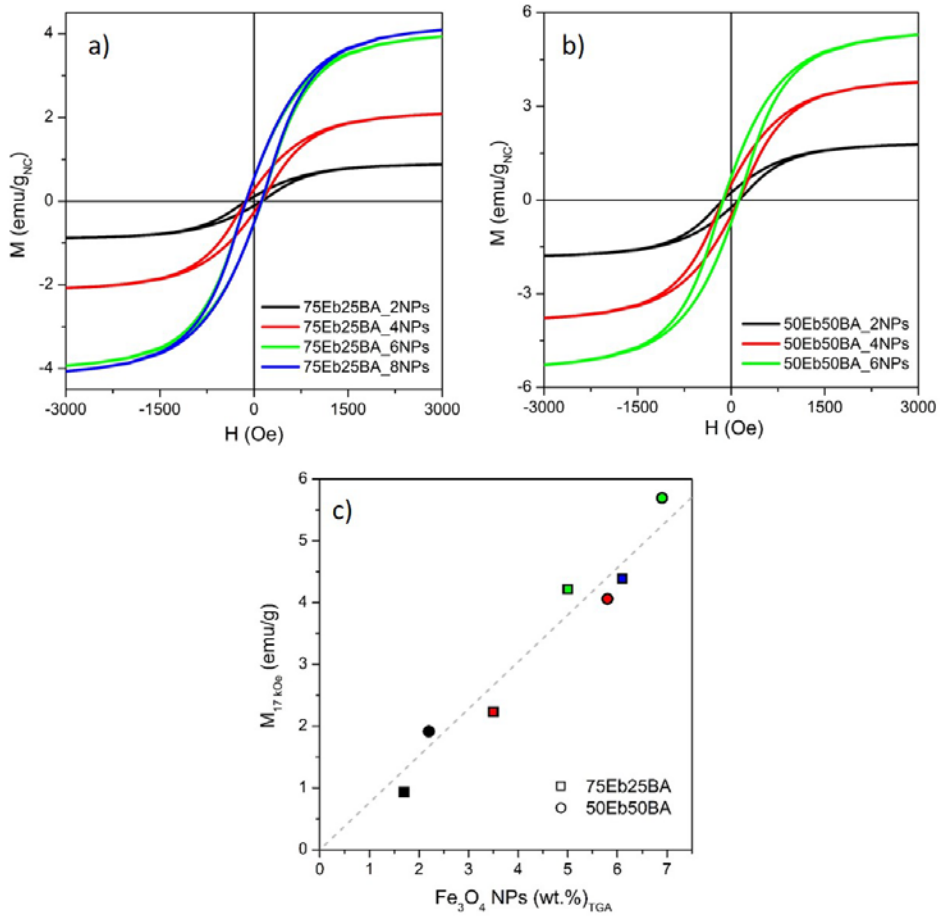

Figure 5. Room temperature hysteresis loops for (a) 75Eb25BA and (b) 50Eb50BA samples at different concentrations; evolution of magnetization (at H = 17 kOe) values for the 3D printed magnetic polymers (75Eb25BA squares and 50Eb50BA circles) as a function of Fe_3O_4 nanoparticles concentration estimated by TGA measurements (dotted line is a guide to the eyes).

3.4 3D Printing

X-Y plane resolution was characterized by printing holes and pillars of progressively smaller dimensions (Figures 6a-c). Moreover, then more complex objects as honeycomb structures were printed to follow the CAD fidelity. Figures 6d-e shows that the printed object reproduces with good fidelity the CAD file. Thus we can state that the maximum resolution obtained for the highest loaded formulations is about 400 µm. At last, to demonstrate the good toughness and flexibility of the final material, we printed thin films, 500 µm thick, and we show that it was possible to bend and twist them without damaging, regardless BA and NPs concentration (Figure S9).

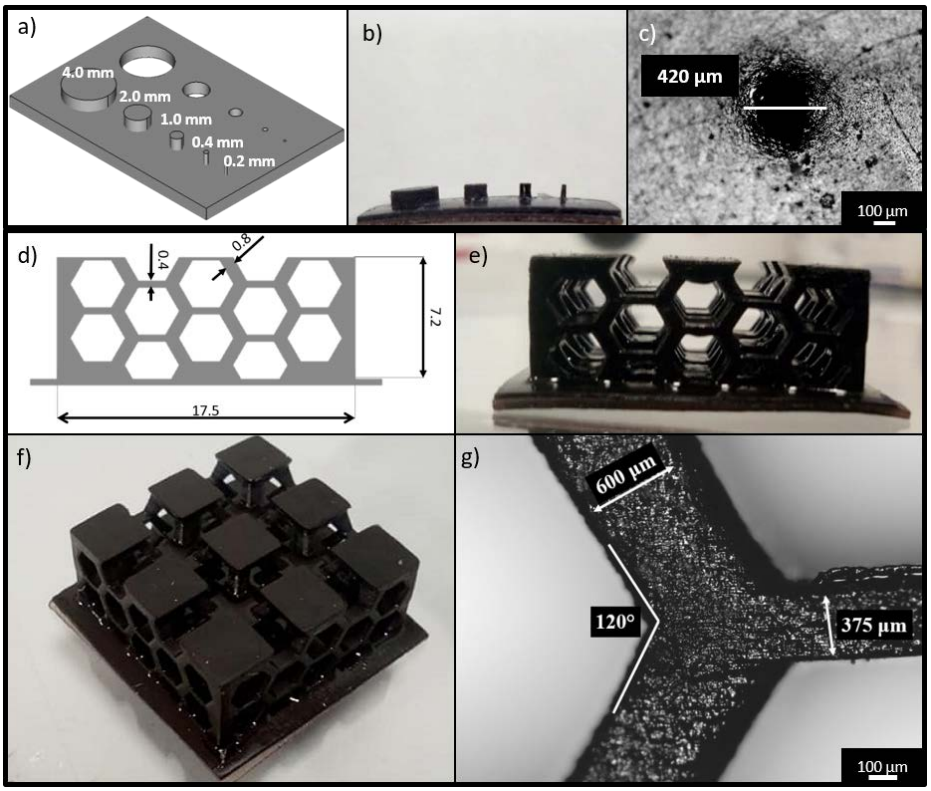

Figure 6: a) CAD design of the object used in order to determine XY resolution on the photocurable resin. b) Image of the corresponding printed object. c) Detail of the hole taken by

optical microscope: scale bar is 100 µm. d) Honeycomb structure CAD file with quotations. e) Lateral face of the printed object. f) Whole printed object. g) Detail of the hexagons taken with optical microscope: scale bar is 100 µm.

Finally, as a proof of concept, we print a set of 3D objects with complex shapes, whose movements can be controlled by applying an external magnetic field. In particular, several types of motion have been investigated: i) rolling, ii) translation, iii) stretching, iv) shape-shifting and v) folding/unfolding. Rolling and translation are the easiest motions to exploit as they are related neither to mechanical properties nor to the shape-shifting of the material but only by the movement of the object as a whole. Thus, in this case, the use of soft and flexible polymeric matrices is not a stringent condition, and the 75Eb25BA formulation, which gives stiffer objects, is perfectly suitable for our purposes. To study the rolling response to an external magnetic field, wheels (Figure 7~~8~~a and Video S1) and spheres (Figure ~~8b~~ 7b and Video S2) have been printed. We note that already at 2 wt.% of nanofiller content, wheels and spheres undergo a rolling motion which is controllable by changing the position of neodymium-iron-boron magnets, whose magnetic field was measured to be about 300 mT. On the other hand, to exploit the translation movement, a cone-like feature was printed and placed in a tube filled with water (Figure ~~8c~~7c). As shown in video S3 in SI, the object can be remotely displaced by applying an external magnetic field.

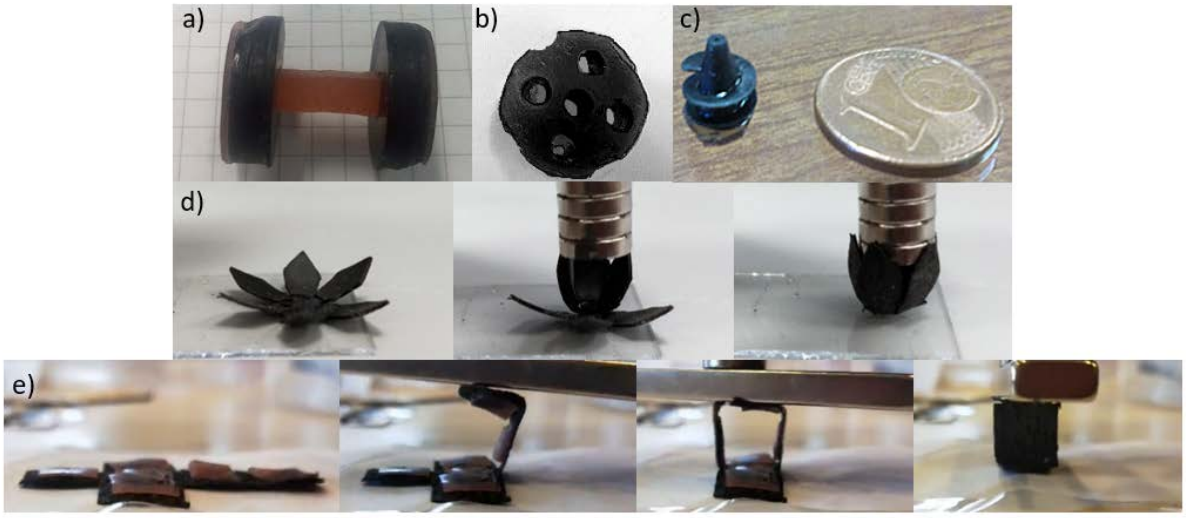

Figure ~~8~~7: 75Eb25BA formulation is used to study rotation and translation movements. a) Printed wheels. b) Printed sphere. c) printed cone-like. d) 50Eb50BA_6NPs flower which encloses itselfwhen exposed to a magnetic field. e) 2D structure composed of flexible and rigid elements able to create a 3D cube when exposed to a magnetic field.

On the other hand, stretching, shape-shifting and folding/unfolding movements need that the printed material is somehow deformed, thus flexibility and softness, which are typical features of soft actuators, are mandatories. In order to produce soft actuators, 50Eb50BA formulation showing lower values of elastic modulus (Figure 3c), cross-linking densities, and glass transition temperatures (Table 2), is preferable to 75Eb25BA formulation, which gives instead stiffer printed objects. To study stretching movements, 50Eb50BA planar springs containing different concentrations of magnetite nanofillers have been printed. As shown in Video S4 and Video S5, when exposed to the same magnetic field (300 mT), the resin 50Eb50BA_6NPs (6 wt% of Fe_2O_3 NPs) shows a larger deformation amplitude than the resin 50Eb50BA_2NPs (2 wt% of $F_{e2}O_3$ NPs). This behavior has a twofold reason: on the one hand, the larger the load of magnetic nanoparticles,

the larger the magnetization of the material and therefore the magnetic force between the printed item and the NdFeB magnets. On the other hand, as previously discussed, the softening of the material scales with the loading of nanofillers. Thus 50Eb50BA_6NPs materials will be more stretchable than 50Eb50BA_2NPs ones. Shapeshifting and folding/unfolding movements are investigated using 50Eb50BA_6NPs formulation as the printed material combines both high toughness and magneto-mechanical response. A flower has been printed to check shape-shifting movement. Figures ~~8d~~ 7d and video S6 in SI) show the blossom-like behavior of the printed flower when exposed to the magnetic field. This example is interesting for several engineering applications such as clamps or holders, as well as for industrial design applications. (*44*) Finally, the combination of polymers bonded magnetic nanofillers and pristine polymer matrices (without magnetic elements) allows the fabrication of a planar structures capable to transform through folding/unfolding movements into a 3D cube (Figure ~~8e~~ 7e and Video S7). Here, pristine polymer elements were insert into the magnetic structure to reinforce the walls of the cube during the folding/unfolding processes.

Conclusions

In this work we report on the fabrication of magneto-responsive nanocomposite polymers using the DLP 3D printing. Photocurable urethane-acrylate resins were loaded with Fe_3O_4 nanoparticles. Mechanical properties of magneto-responsive polymers were tailored, from stiff to soft, by combining urethane-acrylate resins with butyl acrylate reactive diluent, while the magnetic response of the samples was tuned by changing the nanoparticle loading. Besides, we showed that magnetic properties are not affected by the polymer formulation and that the magnetization of the sample is simply proportional to the NPs concentration. The developed formulations were suitable

for 3D printing: he printed objects show high resolution details and fidelity compared to the CAD file, and we were able to print objects up to 6 wt.% of nano-magnetites. For high NPs concentration, i.e. 8 wt%, the competition between photoinitiators and nanofillers in absorbing the the light results in low reactivity and poor mechanical, not allowing the 3D printing process. Finally, several objects with a complex design were printed in 3D by adjusting their mechanical properties and magnetic responses to probe different kind of magnetic-controlled movements: i) rolling, ii) translation, iii) stretching, iv) shape-shifting and v) folding / unfolding.

This study goes in the direction to implement the light-driven printing techniques for the fabrication of high resolution magneto-responsive 3D objects. The possibility to combine the definition associated to the DLP with higher loads of magnetic nanofillers, opens the way to the downscaling of the printing of magneto-responsive items with at the end a board palette of advanced applications ranging from soft-robotics to bio-medicine, from pharmaceutics to flexible electronics.

Acknowledgements

This work is supported by Compagnia di San Paolo through the “Joint Project with Top Universities”.

Bibliography

1. X. Kuang, D.J. Roach, J. Wu, C.M. Hamel, Z. Ding, T. Wang, M.L. Dunn, H.J. Qi, Advances in 4D Printing: Materials and Applications, Adv. Funct. Mater. 29 (2019) 1805290. https://doi.org/10.1002/adfm.201805290

2. A. Mitchell, U. Lafont, M. Hołyńska, C. Semprimoschnig, Additive Manufacturing-A Review of 4D Printing and Future Applications. Add. Manuf. 24 (2018) 6060-626. https://doi.org/10.1016/j.addma.2018.10.038

3. S. Van Hoa, Development of composite springs using 4D printing method. Compos. Struct. 210 (2019) 869-876. https://doi.org/10.1016/j.compstruct.2018.12.003

4. A.B. Baker, S.R. Bates,T.M. Llewellyn-Jones, L.P. Valori, M.P. Dicker, R.S. Trask, 4D printing with robust thermoplastic polyurethane hydrogel-elastomer trilayers. Mater. Design 163 (2019) 107544. https://doi.org/10.1016/j.matdes.2018.107544

5. M. Layani,X. Wang, S. Magdassi, Novel Materials for 3D Printing by Photopolymerization. Adv. Mater. 30 (2018), 1706344. https://doi.org/10.1002/adma.201706344

6. Y. Bar-Cohen, Electroactive polymers as artificial muscles: A review. J. Spacecraft Rockets 39 (2002) 822-827. https://doi.org/10.2514/2.3902

7. T. Mirfakhrai, J.D.W.Madden, R.H. Baughman Polymer artificial muscles Mater. Today. 10 (2007) 30-38. https://doi.org/10.1016/S1369-7021(07)70048-2

8. P. Calvert, Hydrogels for soft machines. Adv. Mater. 21 (2009) 743-756. https://doi.org/10.1002/adma.200800534

9. Z. Liu,P. Calvert, Multilayer hydrogels as muscle-like actuators. Adv. Mater. 12 (2000) 288-291.

10. Kim, S.; Laschi, C.; Trimmer, B., Soft robotics: a bioinspired evolution in robotics. Trends in biotechnology (2013), 31 (5), 287-294. https://doi.org/10.1002/(SICI)1521-4095(200002)12:4<288::AID-ADMA288>3.0.CO;2-1

11. X. Peng,H. Wang, Shape changing hydrogels and their applications as soft actuators. J Polym. Sci. Pol. Phys. 56 (2018) 1314-1324. https://doi.org/10.1002/polb.24724

12. A. Espinha,G. Guidetti,M.C. Serrano, B. Frka-Petesic,A.G. Dumanli, W.Y. Hamad, A. Blanco, C. López, S. Vignolini, Shape memory cellulose-based photonic reflectors. ACS Appl. Mater. Interfaces 8 (2016) 31935-31940. https://doi.org/10.1021/acsami.6b10611

13. M.D. Lima,N. Li,M.J. De Andrade, S. Fang, J. Oh, G.M. Spinks,M.E. KozlovC.S. Haines, D. Suh, J. Foroughi, Electrically, chemically, and photonically powered torsional and tensile actuation of hybrid carbon nanotube yarn muscles. Science 338 (2012), 928-932. https://doi.org/10.1126/science.1226762

14. M. D. Lima,M.W. Hussain,G.M. Spinks,S. Naficy,D. Hagenasr,J.S. Bykova, D. Tolly,R.H. Baughman, Efficient, absorption-powered artificial muscles based on carbon nanotube hybrid yarns. Small 11 (2015), 3113-3138. https://doi.org/10.1002/smll.201500424

15. Z. Cheng, T. Wang, X. Li, Y. Zhang, H. Yu, NIR–Vis–UV light-responsive actuator films of polymer-dispersed liquid crystal/graphene oxide nanocomposites. ACS Appl. Mater. Interfaces 7 (2015) 27494-27501. https://doi.org/ 10.1021/acsami.5b09676

16. L. Hines, K. Petersen,G.Z. Lum, M. Sitti, Soft Actuators for Small-Scale Robotics. Adv. Mater. 29 (2017) 1603483. https://doi.org/10.1002/adma.201603483

17. P. Boyraz,G. Runge,A. Raatz In An Overview of Novel Actuators for Soft Robotics, Actuators, 7 (2018) 48. https://doi.org/10.3390/act7030048

18. B. Gorissen, D. Reynaerts, S. Konishi, K. Yoshida, J.W. Kim, M. De Volder, M., Elastic Inflatable Actuators for Soft Robotic Applications. Adv. Mater. 29 (2017) 1604977. https://doi.org/10.1002/adma.201604977

19. T.Y. Dong, X.I. Zhang, T. Liu, Artificial muscles for wearable assistance and rehabilitation. Front. Inform. Tech. El. 19 (2018) 1303-1315. https://doi.org/10.1631/FITEE.1800618

20. C.Y. Chu,R.M. Patterson, Soft robotic devices for hand rehabilitation and assistance: a narrative review. J. Neuroeng. Rehabil. 15 (2018) 9. https://doi.org/10.1186/s12984-018-0350-6

21. K.E. Peyer, L. Zhang, B.J. Nelson, Bio-inspired magnetic swimming microrobots for biomedical applications. Nanoscale 5 (2013), 5 1259-1272. https://doi.org/10.1039/C2NR32554C

22. D. Grinberg, S. Siddique, M.Q. Le,R. Liang, J.F. Capsal, P.J. Cottinet, 4D Printing based piezoelectric composite for medical applications. J. Polym. Sci. Pol. Phys. 57 (2019) 109-115. https://doi.org/10.1002/polb.24763

23. Y. Kim, H. Yuk, R. Zhao,S.A. Chester, X. Zhao, Printing ferromagnetic domains for untethered fast-transforming soft materials. Nature (2018), 558 (7709), 274. https://doi.org/10.1038/s41586-018-0185-0

24. P. Allia, P. Tiberto, M. Coisson, A. Chiolerio, F. Celegato, F. Vinai, M. Sangermano, L. Suber, G. Marchegiani, Evidence for magnetic interactions among magnetite nanoparticles dispersed in photoreticulated PEGDA-600 matrix. J. Nanopart. Res. 13 (2011), 5615-5626. https://doi.org/10.1007/s11051-011-0249-7

25. T. Nardi, M. Sangermano,Y. Leterrier, P. Allia, P. Tiberto,J.A..E. Månson, UV-cured transparent magnetic polymer nanocomposites. Polymer 54 (2013) 4472-4479. https://doi.org/10.1016/j.polymer.2013.06.052

26. G. Barrera, P. Tiberto, P. Allia, B. Bonelli, S. Esposito, A. Marocco,M. Pansini, Y. Leterrier, Magnetic Properties of Nanocomposites. Appl. Sci.-Basel 9 (2019) 212. https://doi.org/10.3390/app9020212

27. J. Amici, P. Allia, P. Tiberto, M. Sangermano, Poly (ethylene glycol)-Coated Fe3O4 Nanoparticles by UV-Thiol-Ene Addition of PEG Dithiol on Vinyl-Functionalized Magnetite

Surface. Macromol. Chem. Phys. 212 (2011), 1629-1635. https://doi.org/10.1002/macp.201100072

28. J. Amici, M. Kahveci, P. Allia, P. Tiberto, Y. Yagci, M. Sangermano, Polymer grafting onto magnetite nanoparticles by “click” reaction. J. Mater. Sci. 47 (2012) 412-419. https://doi.org/10.1007/s10853-011-5814-z

29. A. Golbang, M. Kokabi, Temporary shape development in shape memory nanocomposites using magnetic force. Eur. Polym. J. 47 (2011) 1709-1719. https://doi.org/10.1016/j.eurpolymj.2011.06.008

30. A. Khosla, B.L. Gray, Micropatternable multifunctional nanocomposite polymers for flexible soft NEMS and MEMS applications. ECS Transactions, 45 2012 477-494. https://doi.org/10.1149/1.3700913

31. D. Kokkinis, M. Schaffner, A.R. Studart, Multimaterial magnetically assisted 3D printing of composite materials. Nat. Commun. 6 (2015) 8643. https:// doi.org/10.1038/ncomms9643

32. A. Bastola, M. Paudel, L. Li, Development of hybrid magnetorheological elastomers by 3D printing. Polymer 149 (2018) 213-228. https://doi.org/10.1016/j.polymer.2018.06.076

33. A. Hodaei, O. Akhlaghi, N. Khani, T. Aytas, D. Sezer, B. Tatli, Y.Z. Menceloglu, B. Koc, O. Akbulut, Single Additive Enables 3D Printing of Highly Loaded Iron Oxide Suspensions. ACS Appl. Mater. Interfaces 10 (2018) 9873-9881. https://doi.org/10.1021/acsami.8b00551

34. H. Fu, K. Nan, W. Bai, W. Huang, K. Bai, L. Lu, C. Zhou, Y. Liu, F. Liu, J. Wang, Morphable 3D mesostructures and microelectronic devices by multistable buckling mechanics. Nat. mater. 17 (2018) 268. https://doi.org/10.1038/s41563-017-0011-3

35. J.A. Cuenca, K. Bugler, S. Taylor, D. Morgan, P. Williams, J. Bauer, A. Porch, Study of the magnetite to maghemite transition using microwave permittivity and permeability

measurements. J. Phys.: Condens. Matter 28 (2016) 106002. https://doi.org/10.1088/0953-8984/28/10/106002

36. F.P.W. Melchels, J. Feijen, D.W. Grijpma, A review on stereolithography and its applications in biomedical engineering. Biomaterials 31 (2010) 6121-6130. https://doi.org/10.1016/j.biomaterials.2010.04.050

37. S. Lantean, I. Roppolo, M. Sangermano, C.F. Pirri, A. Chiappone, Development of New Hybrid Acrylic/Epoxy DLP-3D Printable Materials. Inventions 3 (2018) 29. https://doi.org/10.3390/inventions3020029

38. I. Roppolo, A. Chiappone, A. Angelini, S. Stassi, F. Frascella, C.F. Pirri, C. Ricciardi, E. Descrovi 3D printable light-responsive polymers, Mater. Horiz. 4 (2017) 396-401, . https://doi.org/10.1039/C7MH00072C.

39. M. Hofmann, 3D printing gets a boost and opportunities with polymer materials. ACS Macro Lett 3 (2014) 382-386. https://doi.org/10.1021/mz4006556

40. F. Frascella, G. Gonzalez, P. Bosch, A. Angelini, A. Chiappone, M. Sangermano, C. F. Pirri, I. Roppolo Three-Dimensional Printed Photoluminescent Polymeric Waveguides, ACS Appl. Mater. Interfaces 10 (2018) 39319-39326. https://doi.org/10.1021/acsami.8b16036

41. A. Chiappone, I. Roppolo, E. Naretto, E. Fantino, F. Calignano, M. Sangermano, F. Pirri, Study of graphene oxide-based 3D printable composites: Effect of the in situ reduction. Compos. Part B: Eng. 124 (2017) 9-15. https://doi.org/10.1016/j.compositesb.2017.05.049

42. G. Gonzalez, A. Chiappone, I. Roppolo, E. Fantino, V. Bertana, F. Perrucci, L. Scaltrito, F. Pirri, M. Sangermano, Development of 3D printable formulations containing CNT with enhanced electrical properties. Polymer 109 (2017) 246-253. https://doi.org/10.1016/j.polymer.2016.12.051

43. J.J. Martin, B.E. Fiore, R.M. Erb, Designing bioinspired composite reinforcement architectures via 3D magnetic printing. Nat. Comm. 6 (2015) 8641. https://doi.org/10.1038/ncomms9641

44. Z. Ji, C. Yan, B. Yu, X. Wang, F. Zhou, Multimaterials 3D Printing for Free Assembly Manufacturing of Magnetic Driving Soft Actuator. Adv. Mater. Interf. 4 (2017) 1700629. https://doi.org/10.1002/admi.201700629

45. M. Sangermano, W. Carbonaro, G. Malucelli, A. Priola, UV-Cured Interpenetrating Acrylic-Epoxy Polymer Networks: Preparation and Characterization. Macromol. Mater. Eng. 293 (2008) 515-520. https://doi.org/10.1002/mame.200800020

46. K.D. Jandt, R.W. Mills A brief history of LED photopolymerization. Dent. Mater. 29 (2013) 605-617. https://doi.org/10.1016/j.dental.2013.02.003

47. J. Fouassier, X. Allonas, D. Burget, Photopolymerization reactions under visible lights: principle, mechanisms and examples of applications. Progr. org. coat. 47 (2003) 16-36. https://doi.org/10.1016/S0300-9440(03)00011-0

48. O. Valdes-Aguilera, C. Pathak, J. Shi, D. Watson, D. Neckers, Photopolymerization studies using visible light photoinitiators. Macromolecules 25 (1992) 541-547. https://doi.org/10.1021/ma00028a008

49. A. Schlegel, S. F. Alvarado, P. Wachter, Optical properties of magnetite (Fe3O4), J. Phys. C: Solid State Phys 12 (1979) 1157

50. M. Fernández–García, R. Cuervo–Rodriguez, E. Madruga, Glass transition temperatures of butyl acrylate–methyl methacrylate copolymers. J Polym. Sci. Pol. Phys. 37 (1999) 2512-2520. https://doi.org/10.1002/(SICI)1099-0488(19990901)37:17<2512::AID-POLB22>3.0.CO;2-2

51. C. Gao, Y. Wang, D. Hu, Z. Pan, L. Xiang Tribological properties of magnetite nanoparticles with various morphologies as lubricating additives. J. nanopart. res. 15 (2013) 1502. https://doi.org/10.1007/s11051-013-1502-z

52. G. Herzer Grain size dependence of coercivity and permeability in nanocrystalline ferromagnets. IEEE T. Magn 26 (1990) 1397-1402. https://doi.org/10.1109/20.104389